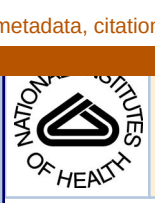

Published in final edited form as:
Cell Stem Cell. 2014 December 4; 15(6): 707–719. doi:10.1016/j.stem.2014.09.019.

m^{6}A RNA modification controls cell fate transition in mammalian embryonic stem cells

Pedro J Batista[1,*], **Benoit Molinie**[2,*], **Jinkai Wang**[3,*], **Kun Qu**[1], **Jiajing Zhang**[1], **Lingjie Li**[1], **Donna M Bouley**[4], **Ernesto Lujan**[5,6], **Bahareh Haddad**[5], **Kaveh Daneshvar**[2], **Ava C Carter**[1], **Ryan A Flynn**[1], **Chan Zhou**[2], **Kok-Seong Lim**[7], **Peter Dedon**[7], **Marius Wernig**[5], **Alan C Mullen**[2,8], **Yi Xing**[3,¶], **Cosmas C Giallourakis**[2,8,¶], and **Howard Y Chang**[1,¶]

[1]Howard Hughes Medical Institute and Program in Epithelial Biology, Stanford University School of Medicine, Stanford, CA 94305, USA

[2]Gastrointestinal Unit, Massachusetts General Hospital, Harvard Medical School, Boston, MA 02114, USA

[3]Department of Microbiology, Immunology, and Molecular Genetics, University of California, Los Angeles. CHS 33–260, 650 Charles E. Young Drive South, Los Angeles, CA 90095, USA

[4]Department of Comparative Medicine, Stanford University School of Medicine, Stanford, CA 94305, USA

[5]Institute for Stem Cell Biology and Regenerative Medicine and Department of Pathology, Stanford, CA 94305, USA

[6]Department of Genetics, Stanford, CA 94305, USA

[7]Massachusetts Institute of Technology Department of Biological Engineering, 56–787b 77 Massachusetts Ave. Cambridge, MA 02139, USA

[8]Harvard Stem Cell Institute, Cambridge, MA 02138, USA

SUMMARY

N6-methyl-adenosine (m^{6}A) is the most abundant modification on messenger RNAs and is linked to human diseases, but its functions in mammalian development are poorly understood. Here we

¶Correspondence to: H.Y.C. (howchang@stanford.edu), C.C.G. (CGIALLOURAKIS@mgh.harvard.edu), and Y.X. (yxing@ucla.edu).
*Co-first authors.

Author contributions

PJB and HYC conceived of the mESC studies; PJB, LL, DMB, EL, ACC, RAF, MW, YX and HYC designed and performed experiments in the mouse system. ACM, YX, CCG conceived of the hESC studies; BM, BH, KD, CZ, KL, PD, MW, ACM, YX, CCG designed and performed experiments in the human system. JW, KQ, JZ analyzed the data. PJB, BM, JK, YX, CCG and HYC wrote the paper with input from all authors.

Accession Numbers

The accession number for the RNA sequencing are: GSE52681 (mouse) and GSE52600 (human).

reveal the evolutionary conservation and function of m^{6}A by mapping the m^{6}A methylome in mouse and human embryonic stem cells. Thousands of messenger and long noncoding RNAs show conserved m^{6}A modification, including transcripts encoding core pluripotency transcription factors. m^{6}A is enriched over 3′ untranslated regions at defined sequence motifs, and marks unstable transcripts, including transcripts turned over upon differentiation. Genetic inactivation or depletion of mouse and human *Mettl3*, one of the m^{6}A methylases, led to m^{6}A erasure on select target genes, prolonged *Nanog* expression upon differentiation, and impaired ESC's exit from self-renewal towards differentiation into several lineages in vitro and in vivo. Thus, m^{6}A is a mark of transcriptome flexibility required for stem cells to differentiate to specific lineages.

INTRODUCTION

Reversible chemical modifications on messenger RNAs have emerged as prevalent phenomena that may open a new field of "RNA epigenetics", akin to the diverse roles that DNA modifications play in epigenetics (reviewed by (Fu and He, 2012; Sibbritt et al., 2013)). N6-methyl-adenosine (m^{6}A) is the most prevalent modification of mRNAs in somatic cells, and dysregulation of this modification has already been linked to obesity, cancer, and other human diseases (Sibbritt et al., 2013). m^{6}A has been observed in a wide range of organisms, and the methylation complex is conserved across eukaryotes. In budding yeast, the m^{6}A methylation program is activated by starvation and required for sporulation. In *Arabidopsis thalania*, the methylase responsible for m^{6}A modification, MTA, is essential for embryonic development, plant growth and patterning, and the Drosophila homolog IME4 is expressed in ovaries and testes and is essential for viability (reviewed in (Niu et al., 2013)).

While m^{6}A has been suggested to affect almost all aspects of RNA metabolism, the molecular function of this modification remains incompletely understood (Niu et al., 2013). Importantly, m^{6}A modification(s) are reversible in mammalian cells. Two members of the alpha ketoglutarate-dependent dioxygenases protein family, fat-mass and obesity associated protein (FTO) and ALKBH5 have been shown to act as m^{6}A demethylases (Jia et al., 2011; Zheng et al., 2013). Manipulating global m^{6}A levels has implicated m^{6}A modifications in a variety of cellular processes including nuclear RNA export, control of protein translation and splicing (reviewed in (Meyer and Jaffrey, 2014)). Recently, m^{6}A modification has been suggested to play a role in controlling transcript stability as YTH domain family of "reader" proteins specifically bind m^{6}A sites and recruit the transcripts to RNA decay bodies (Kang et al., 2014; Wang et al., 2014a).

Whereas the DNA methylome undergoes dramatic reprogramming during early embryonic life, the developmental origins and functions of m^{6}A in mammals are incompletely understood. Furthermore, the degree of evolutionary conservation of m^{6}A sites is not known in ESCs. To date, the functions of m^{6}A in mammalian cells have only been examined by RNAi knockdown. Depletion of METTL3 and METTL14 in human cancer cell lines led to decreased cell viability and apoptosis, leading to the interpretation that m^{6}A is important for cell viability (Dominissini et al., 2012; Liu et al., 2014). A recent study reported that depletion of Mettl3 inhibited mouse ESC proliferation and led to ectopic differentiation

(Wang et al., 2014b). Here we assess the conservation of the m^{6}A methylome at the level of gene targets and function in mouse and human ESCs. We report the consequences of genetic ablation of Mettl3 in mouse ESCs (mESCs) as well as depletion of METTL3 in human ESCs (hESCs). These experiments led to the unexpected finding that m^{6}A and Mettl3 in particular are not required for ESC growth but are required for stem cells to adopt new cell fates.

RESULTS

Thousands of mESC transcripts bear m^{6}A

To understand the role of the m^{6}A RNA modification in early development, we mapped the locations of m^{6}A modification across the transcriptome of mouse (mESC) and human (hESC) embryonic stem cells by m^{6}A RIP-seq as described. (Dominissini et al., 2012; Meyer et al., 2012) (Methods). For each experiment, libraries were built for multiple biological replicates and concordant peaks for each experiment were used for subsequent bioinformatic analyses.

In mESCs, m^{6}A-seq revealed a total of 9754 peaks in 5578 transcripts (average 2 peaks per transcript), including 5461 mRNAs (of 9923 mRNAs) and 117 lncRNAs. Due to the lower expression levels of lncRNA as a class, our approach likely underestimates the fraction of modified noncoding transcripts (Table S1). Thus, thousands of mESC transcripts, including mRNAs and lncRNAs, are m^{6}A modified.

m^{6}A in mRNAs of mESC core pluripotency factors

We found that mRNAs encoding the core pluripotency regulators in mESCs were modified with m^{6}A (Dunn et al., 2014; Young, 2011), including *Nanog, Klf4, Myc*, *Lin28, Med1*, *Jarid2* and *Eed*, whereas *Pou5f1* (also known as *Oct4*) lacked m^{6}A modification (Figure 1A, B). We confirmed m^{6}A-seq results with independent m^{6}A IP-qRT-PCR. (Figure S1A) and m^{6}A-IP followed by Nanostring nCounter analysis (m^{6}A-string) (Table S2). These validation results suggest that the m^{6}A-seq data are accurate and robust. The top group of modified genes, based on degree of modification, was enriched for several functional groups, including: chordate embryonic development, embryonic development, gastrulation and cell cycle (Figure 1C). Thus, in mESCs, m^{6}A targets include the ESC core pluripotency network and transcripts with dynamically controlled abundance during differentiation.

m^{6}A location and motif in mESCs suggest a common mechanism shared with somatic cells

De novo motif analysis of mESC m^{6}A sites specifically identified the previously described RRACU m^{6}A sequence motif in somatic cells (Figure 1D, S1B) (reviewed in (Meyer and Jaffrey, 2014)). Furthermore, like somatic cells, m^{6}A sites in mESC are significantly enriched near the stop codon and beginning of the 3′ UTR of protein coding genes (Figure 1E and 1F), as previously described for somatic mRNAs. Although the largest fraction of m^{6}A sites was within the coding sequence (CDS, 35%), the stop codon neighborhood is most enriched, comprising 33% of m^{6}A sites while representing 12% of the motif occurrence. In genes with only one modification site, this bias is even more pronounced

(Figure 1F). Comparison of transcript read coverage between input and wild type revealed no bias for read accumulation around the stop codon in the input sample (Figure S1C).

In addition to the last exon, which often includes the stop codon and 3′-UTR, we found a strong bias for m^{6}A modification occurring in long internal exons (median exon length of 737bp vs. 124 bp; $P<2.2\times10^{-16}$; two-sided Wilcoxon test), even when the number of peaks per exon was normalized for exon length or motif frequency (Figure S1D–F). These results suggest the possibility that processing of long exons is coupled mechanistically to m^{6}A targeting through as yet unclear systems and/or that m^{6}A modification itself may play a role in controlling long exon processing. The topological enrichment of m^{6}A peaks surrounding stop codons in mRNAs is a poorly understood aspect of the m^{6}A methylation system. We sought to understand if there was a topological enrichment or constraint on m^{6}A modification in non-coding RNAs (ncRNAs), which lack stop codons. We parsed both classes of RNAs with three or more exons into three normalized bins including the 1st, all internal and last exon. We observed an enrichment of m^{6}A near the last exon-exon splice junction for both coding and ncRNAs and toward 3′ end of single-exon genes (Figure 1G, S1G–H), suggesting that the 3′ enrichment of m^{6}A peaks can occur independently of translation or splicing. Together, the location and sequence features we identified in mESCs suggest a mechanism for m^{6}A deposition that is similar if not identical in somatic cells.

m^{6}A is a mark for RNA turnover

We next tested if transcript levels are correlated with the presence of m^{6}A modification. Comparison of m^{6}A enrichment level versus the absolute abundance of RNAs revealed no correlation between level of enrichment and gene expression (Figure 1H). A separate, quartile based analysis found a higher percentage of m^{6}A-modified transcripts in the middle quartiles of transcript abundance (Figure S1I). Thus, our analysis suggests that m^{6}A modification is not simply a random modification that occurs on abundant cellular transcripts; rather, m^{6}A preferentially marks transcripts expressed at a medium level.

To further define potential mechanisms of m^{6}A function, we asked whether m^{6}A-marked transcripts differ from unmodified transcripts at the level of transcription, RNA decay, or translation by leveraging published genome-wide datasets in mESCs. RNA polymerase II occupancy at the promoters encoding both unmodified and m^{6}A-marked RNAs is similar (Figure S1J). In contrast, m^{6}A-marked transcripts had significantly shorter RNA half-life — 2.5 hours shorter on average ($p= < 2.2^{-16}$, Figure 1I), and increased rate of mRNA decay (average decay rate of 9 min vs. 5.4 min for m^{6}A vs. unmodified, $p= < 2.2^{-16}$). m^{6}A modified transcripts have slightly lower translational efficiency than unmodified transcripts (1.32 vs. 1.51, respectively) (Ingolia et al., 2011) (Figure S1K). These results suggest that m^{6}A is a chemical mark associated with transcript turnover.

Mettl3 knockout decreases m^{6}A and promotes ESC self-renewal

To understand the role of m^{6}A methylation in ESC biology, we chose to inactivate *Mettl3*, encoding one of the components of the m^{6}A methylase complex. To date no genetic study of *Mettl3* has been performed to rigorously define its requirement for m^{6}A modification, as all studies have relied on knock down. We targeted *Mettl3* by CRISPR-mediated gene editing,

and generated several homozygous *Mettl3* Knockout (KO) mESC lines. DNA sequencing confirmed homozygous stop codons that terminate translation within the first 75 amino acids, and immunoblot analysis confirmed the absence of Mettl3 protein (Figure 2A, Figure S2A). Two dimensional thin layer chromatography (2D-TLC) showed a significant (~60%) but incomplete reduction of m^6A in *Mettl3* KO mESC (Figure 2B and Figure S2B). Contrary to a recent publication (Wang et al., 2014b), Mettl3 KO slightly reduced but did not prevent the stable accumulation of Mettl14 (Figure S2C). These experiments provide formal genetic proof that Mettl3 is a major, but not the sole, m^6A methylase in mESC.

Contrary to the expectation in the literature, the *Mettl3* KO mESCs are viable and surprisingly demonstrated improved self-renewal. *Mettl3* KO mESCs could be maintained indefinitely over months and exhibited low levels of apoptosis, similar to wild type mESCs, as judged by PARP cleavage and Annexin V flow cytometry (Figure 2A, Figure S2D). We next asked whether *Mettl3* KO affected the ability of stem cells to remain pluripotent. *Mettl3* KO mESC colonies were consistently larger than WT ESCs, and retained the round, compact ESC colony morphology with intense alkaline phosphatase staining comparable to wild type colonies as well as uniform expression of Nanog and Oct4 (Figure 2C, 2D, 2E, Figure S2E and data not shown). Quantitative cell proliferation assay confirmed the increased proliferation rate of KO over WT mESCs (Figure 2F). These observations suggest that *Mettl3* KO enables enhanced mESC self-renewal. To rule out potential off-target effects from CRISPR-mediated gene targeting, we used an orthogonal approach to knockdown Mettl3 in mESCs. Two independent short hairpin RNAs (shRNAs) knocked down Mettl3 to ~20% (Figure S2F). 2D-TLC showed a ~40% loss of m^6A in poly(A) RNAs (Figure S2G), and apoptosis assays confirmed lack of cell death induction. Importantly, Mettl3 depletion also increased mESC proliferation compared to control shRNA for one hairpin (Figure S2H). Thus, two independent approaches confirm that *Mettl3* inactivation enhanced self-renewal of ESCs.

Mettl3 KO blocks directed differentiation in vitro and teratoma differentiation in vivo

These findings, coupled with the observation that modified genes tend to have a shorter half-life, suggest that Mettl3, and by extension m^6A, is needed to fine-tune and limit the level of many ESC genes, including pluripotency regulators. Since Mettl3 KO cells are capable of self-renewal, we tested their capacity for directed differentiation *in vitro* toward two lineages: cardiomyocytes (CM) and the neural lineage. While the WT cells were able to generate beating CM (~50% of colonies), only ~3% of Mettl3 KO colonies of two independent clones produced beating CMs. Furthermore, differentiated colonies of Mettl3 KO cells retained high levels of *Nanog* expression but lacked expression of the CM structural protein Myh6, reflecting a larger number of cells that failed to exit the mESC program in the mutant cells. (Figure 3A and Supplemental Video 1 and 2). Similarly, upon directed differentiation to the neural lineage, we observed a marked difference between the ability of the two cells types to differentiate. To assay for neural differentiation we stained for Tuj1, a beta-3 tubulin expressed in mature and immature neurons. While ~53% of wild type colonies had Tuj1+ projections, less than 6% of Mettl3 KO colonies had Tuj1+ projections in both KO clones (Figure 3B). Additionally, differentiated *Mettl3* KO cells showed an impaired ability to repress *Nanog* and activate Tuj1 mRNA (Figure 3B). To

confirm the role of Mettl3 in mESC differentiation *in vivo*, we injected *Mettl3* KO or wild type cells subcutaneously into the right or left flank respectively, of SCID/Beige mice (n=5). Both wild type and *Mettl3* KO cells formed tumors consistent in morphology with teratomas. Mutant tumors tended to be larger, in accordance with mutant cell growth curves observed *in vitro* (Figure 3C). Histological analysis of H&E stained tumor sections revealed consistent differences between the two populations. While both groups of cells formed teratomas that contained some degree of differentiation into all three germ layers, the teratomas derived from KO cells were predominantly composed of poorly differentiated cells with very high mitotic indices and numerous apoptotic bodies, whereas wild type cells differentiated predominantly into neuroectoderm (Figure 3D). Analysis of adjacent sections revealed that the mutant teratomas have markedly higher staining of proliferation marker Ki67 and ESC protein Nanog, which highlight the poorly differentiated cells (Figure 3E, 3F and Figure S3A). *Mettl3* KO tumors had higher levels of *Nanog*, *Oct4* and *Ki67* mRNAs and lower levels of *Tuj1*, *Myh6* and *Sox17* mRNAs (Figure S3B). These results suggest that insufficient m^6A leads to a block in ESC differentiation and persistence of a stem-like, highly proliferative state.

Mettl3 target genes in mESCs

The incomplete loss of bulk m^6A in Mettl3 KO may result because Mettl3 is solely responsible for the methylation of a subset of genes or sites and/or Mettl3 functions in a redundant fashion with another methylase on all m^6A-modified genes. To distinguish these possibilities, we mapped the m^6A methylome in Mettl3 KO cells. Comparison of the methylomes of wild type vs. Mett3 KO mESCs revealed a global loss of methylation across m^6A sites identified in wild type (Figure 4A). We detected changes in 3739 sites (in 3122 genes), including modification sites in *Nanog* mRNA. Thus, this unbiased analysis suggested a set of targets that rely more exclusively on Mettl3, including *Nanog* and other pluripotency mRNAs (Figure 4B and 4C) (Table S1). Gene Set Enrichment Analysis confirmed that Mettl3-target genes significantly overlap functional gene sets important for pluripotency, including *targets of Ctnnb1* (4.43×10^{-6}), *targets of Smad2 or Smad3* (1.03×10^{-16}), *targets of Myc* (9.20×10^{-10}), *targets of Sox2* (4.75×10^{-8}), and *targets of Nanog* (7.18×10^{-8}) (Figure 4C), and include five of eleven core ESC regulators such as *Nanog*, *Rlf1*, *Jarid2*, and *Lin28* (Figure 4D). Independent validation by m^6A RIP followed by Nanostring detection confirmed loss of m^6A in *Nanog* and other mRNAs in KO vs. wild type mESCs (Figure 4E). Further, following transcription arrest by flavopiridol treatment, *Nanog* mRNA showed delayed turnover in Mettl3 KO cells compared to wild type, consistent with a requirement for m^6A in *Nanog* mRNA turnover (Figure 4F). However, RNA-seq analysis of Mettl3 KO cells revealed modest perturbations in mRNA steady state levels with only ~300 genes demonstrating significant changes over 1.5 fold. Collectively, these results suggest ESC genes are under Mettl3 control, and m^6A impacts ESC biology.

Wide spread m^6A modification of human ESCs

The identification of thousands of m^6A sites raises the challenge of defining the functional importance of each and every one of the sites. We reasoned that evolutionary conservation provides a powerful and comprehensive metric of function. To this end, we mapped m^6A sites in hESCs and during endoderm differentiation to elucidate the patterns and potential

conservation of m^{6}A methylome (Figure 5A). In basal state hESCs (Time (T) = 0), m^{6}A-seq identified 16943 peaks in 7871 genes representing 7530 coding and 341 non-coding RNAs. Upon differentiation towards endoderm (T = 48, "endoderm differentiation" thereafter), m^{6}A-seq identified 15613 m^{6}A peaks in 7195 genes representing 6909 coding and 286 non-coding RNAs (Table S3). As shown in Figure 5B, 11322 peaks (6004 genes) were common between the undifferentiated and differentiated hESCs, while 5348 (3979 genes) vs. 4087 peaks (3024 genes) were unique, respectively.

Many master regulators of hESC maintenance and differentiation are modified with m^{6}A

As we observed for mESC, transcripts encoding many hESC master regulators, including human NANOG, SOX2, and NR5A2, were m^{6}A modified. Like mESC, the transcripts for OCT4 (POUF51) in hESC did not harbor an m^{6}A modification (Figure 5D). These results show that in both organisms the core-pluripotency/maintenance genes are under the regulatory influence of the m^{6}A pathway. We also identified human specific lncRNAs with known roles in hESC maintenance such as LINC-ROR and *MEGAMIND/TUNA* to contain m^{6}A modification(s) (Figure 5D; Figure S4A) (Lin et al., 2014; Loewer et al., 2010). Upon induction of differentiation, we observed transcripts encoded by several key regulators of endodermal differentiation also to have m^{6}A modifications including EOMES and FOXA2 (Figure 5D). Gene ontology (GO) analyses of methylated genes in undifferentiated hESCs, and after endodermal differentiation, were significantly enriched in biological functions such as *regulation of transcription* (FDR=1.2×10^{-14}), *chordate embryonic development* (FDR=1.1×10^{-4}), and *regulation of cell morphogenesis* (FDR=0.01).

Upon differentiation toward endoderm, 1356 peaks in 1137 genes showed quantitative differences of at least 1.5 fold in m^{6}A intensity, after normalization for input transcript abundance (Figure 5E and 5F, Table S4). The majority of these differential m^{6}A sites represented quantitative differences at existing sites (i.e. 59.1% of the peaks were called in both time points), rather then state-specific *de novo* appearance or erasure of modification (Figure 5G). This is consistent with the observation that 74.9% of sites in the hESCs overlapped those observed in HEK293T data (Meyer et al., 2012) and the minimal changes in m^{6}A sites observed in a recent survey of m^{6}A pattern across cell types (Schwartz et al., 2014). We suggest that transcripts exhibit dynamic differential peak m^{6}A methylation intensity largely at "hard wired sites" during differentiation under the conditions examined and when compared to other tissue types.

Conserved features of m^{6}A modifications spanning different species

We found that three salient features of the m^{6}A methylome are conserved in hESCs. First, m^{6}A sites in hESCs are also dominated by the RRACU motif seen in mESC and somatic cells (Dominissini et al., 2012; Meyer et al., 2012) (Figure 5C). There was also a strong preference of targeting long-internal exons at the RRACU motif even after normalizing for exon length and number of m^{6}A motifs (Figure 5H). Second, there was a significant enrichment in m^{6}A peaks at 3′ end of transcripts, near the stop codon of coding genes or the last exon in non-coding RNAs (Figure 5I, Figure S4B, S4C and S4D). Furthermore, the topology of m^{6}A modification is preserved upon endodermal differentiation (Figure 5I). As in mESCs, moderate to lowly expressed genes have higher probability of becoming

methylated (Figure S4E). Lastly, hESC m^6A is not correlated with transcription rate as judged by GRO-seq (Sigova et al., 2013), but is strongly anti-correlated with measured mRNA half-life in human pluripotent cells (Neff et al., 2012), strongly suggesting that m^6A modification also marks RNA turnover in hESCs (Figure 5J, Figure S4F and S4G).

Evolutionary conservation and divergence of the m^6A epi-transcriptomes of human and mouse ESCs

Previous studies suggested significant conservation of m^6A modified genes between mouse and human in somatic cell types, but the comparisons are limited by non-matched tissue types (Dominissini et al., 2012; Meyer et al., 2012). We were thus interested in examining the evolutionary conservation of human and mouse ESC m^6A methylomes. At the gene level, 69.4% (3609 of 5204) of hESC genes are also m^6A modified in the orthologus mouse gene (p-value= 8.3×10^{-179}; Fisher exact test) (Figure 6A; Table S5). Furthermore, we identified 632 conserved m^6A peak sites (46.1%) between hESCs and mESCs (Table S6). Notably, conserved sites tended to have higher m^6A peak intensities compared to m^6A peak sites that are not conserved (Figure 6B and 6C, *p*-values=1.3×10^{-15} and 8.7×10^{-23} for hESC or mESC, respectively; Wilcoxon test). Commonly methylated genes can demonstrate m^6A modification sites at identical site(s) such as GLI1, similar but not identical locations such as SOX2, or m^6A site at different exons, such as CHD6 (Figure 6D, 6E and 6F, Table S4). Our data thus reveal a substantial overlap at the gene level, suggesting broad functional significance of m^6A modification in ESCs in both species. At the same time, we also observed numerous species-specific m^6A patterns that may contribute to specific aspects of ESC biology (Schnerch et al., 2010).

METTL3 is required for hESC differentiation

To address the function of m^6A in hESCs, we generated hESC colonies with stable knockdown of METTL3 and shRNA control (Figure 7A). Knockdown of METTL3 in hESCs resulted in reduction in METTL3 mRNA levels and reduction in m^6A level (Figure 7B, 7C and Figure S5B, S5C). METTL3-depleted hESCs could be stably maintained, suggesting the dispensability of METTL3 for hESC self-renewal or viability. Strikingly, differentiation of METTL3-depleted hESCs into neural stem cells (NSCs) by dual inhibition of SMAD signaling, using Dorsomorphin and SB-431542 revealed a block in neuronal differentiation (Methods). While 44% (+/−3.5% s.d.) of the control cells were Sox1 positive, only 10% (+/−3.1% s.d) of the METTL3-depleted were Sox1 positive (Figure S5A).

Similarly, knockdown of METTL3, in three independently generated hES colony clones selected for METTL3 knockdown, led to a profound block in endodermal differentiation at day 2 and day 4 based on failure to express the endoderm markers *EOMES* and *FOXA2* compared to either two shRNA control colony clones (Figure 7D) or wildtype hESCs (Figure S5D). Consistently, METTL3-depleted ESCs retain high levels of expression of the master regulators *NANOG* and *SOX2* throughout the differentiation time course in contrast to their diminishing expression in wild type cells (Figure 7E and S5E). These results indicate that METTL3 and m^6A control differentiation of human embryonic stem cells.

DISCUSSION

m^{6}A methylome in ES cells

Our analysis of the ESC m^{6}A methylome in mouse and human cells reveals extensive m^{6}A modification of ESC genes, including most key regulators of ESC pluripotency and lineage control. However, this observation does not mean that m6A is uniquely tied to the pluripotency network. Because m6A marks moderately expressed transcripts that need to be turned over in a timely fashion, such genes in ESCs likely include many regulators of pluripotency and lineage determination. The pattern and sequence motif associated with ESC m^{6}A are similar if not identical to those previously reported in somatic cells, suggesting a single mechanism that deposits m^{6}A modification in early embryonic life. This invariant mechanism for m^{6}A contrasts with the complexity of 5-methyl-cytosine in DNA and histone lysine methylations that undergo extensive reprogramming with distinct rules in pluripotent vs. somatic cells.

We identified a general and conserved topological enrichment of m^{6}A sites at the 3′ end of genes among single-exon and multi-exon mRNAs as well as ncRNAs. Thus, neither the stop codon nor the last exon-exon splice junction can alone explain the observed m^{6}A topology in RNA. However, all species examined to date including *Saccharomyces cerevisae* and *A. thalania* exhibit a strong 3′ bias in m^{6}A localization, suggesting an evolutionary constraint that may target the m^{6}A modification to the 3′ ends of genes regardless of gene structure or coding potential. This bias may be achieved by preferential m^{6}A methylases recruitment to 3′ sites or preferential action of demethylases in upstream regions of the transcript. Although the role of demethylases cannot be excluded, the observation of 3′ end m^{6}A bias in *S. cerevisiae*, which lacks known m^{6}A demethylases argues against the latter mechanism (Bodi et al., 2012; Jia et al., 2011; Schwartz et al., 2013; Zheng et al., 2013). The functional importance of m^{6}A location vs. its specific molecular outcome need to be addressed in future studies.

Mettl3 selectively targets mRNAs including pluripotency regulators

While several studies had approached Mettl3 function by RNAi knock down (Dominissini et al., 2012; Fustin et al., 2013; Liu et al., 2014; Wang et al., 2014b), genetic ablation of *Mettl3* KO allowed us to examine the true loss-of-function phenotypes. The importance of using definitive genetic models is highlighted by recent studies in the DNA methylation field where shRNA experiments led to mis-assigned functions of Ten-eleven translocation (TET) proteins that were later recognized in genetic knockouts (Dawlaty et al., 2013; Dawlaty et al., 2011). We found that both *Mettl3* KO and depletion led to incomplete reduction of the global levels m^{6}A in both mESCs and hESCs, demonstrating redundancy in m^{6}A methylases. However, m^{6}A profiling in Mettl3 KO cells revealed a subset of targets, approximately 33% of m^{6}A peaks, that are preferentially dependent on Mettl3, and these included *Nanog*, *Sox2*, and additional pluripotency genes. A second m^{6}A methylase, Mettl14, was described during the preparation of this manuscript.

RNAi knockdown of Mettl3 in somatic cancer cells led to apoptosis (Dominissini et al., 2012), and one study reported ectopic differentiation of mESC with Mettl3 depletion (Wang

et al., 2014b). In contrast, we found that Mettl3 KO does not affect mESC cell viability or self-renewal, and in fact mESC renewed at an improved rate. The differences in phenotype observed could potentially be explained by different dependency on m^6A modified RNAs in different cell types, acute versus chronic inactivation, or RNAi off target effects. m^6A methylome analysis in different cell types with Mettl3 inactivation may shed light on these differences in the future.

Conservation of m6A methylome in mammalian ESCs

The conserved methylation patterns of many ESC master regulators and the shared phenotype observed upon inactivation of METTL3 suggest that METTL3 operates to control stem cell differentiation. It is known that human and mouse ESCs are not equivalent (Schnerch et al., 2010), and are cultured in different conditions. By focusing in on orthologous genes, we were able to catalog both shared and species-specific methylation sites. The observation that certain methylation sites are modified whenever a target transcript is expressed in both species, despite cell state or culture differences, argues that these modification events have been preserved under strong purifying selection during evolution. Our comparative genomic analyses also pave the way to further understand potential biological differences between mouse and human ESCs at the level of m^6A epitranscriptome, given the unique patterns of some methylation sites between the species.

RNA “anti-epigenetics”: m^6A as a mark of transcriptome flexibility

Stem cell gene expression programs need to balance fidelity and flexibility. On one hand, stem cell genes need sufficient stability to maintain self-renewal and pluripotency over multiple cell generations, but on the other hand, gene expression needs to change dynamically and rapidly in response to differentiation cues. It has been proposed that ESC gene expression programs are in constant flux between competing fates, and pluripotency is a statistical average (Loh and Lim, 2011; Montserrat et al., 2013; Shu et al., 2013). We found that mRNAs with m^6A tend to have a shorter half-life, and *Nanog* and *Sox2* mRNAs could not be properly down-regulated with differentiation in Mettl3-deficient mESC and hESC. However, Mettl3 deficiency has only modest effects on steady state gene expression, which could arise from the non-stoichiometric nature of the m^6A modification. The application of methods that can determine level of modification of each RNA species will allow us to answer these questions (Harcourt et al., 2013; Liu et al., 2013). *Mettl3* KO mESCs have enhanced self-renewal but hindered differentiation, concomitant with decreased ability to down regulate ESC mRNAs. WTAP, a conserved Mettl3 interacting partner from yeast to human cells (Horiuchi et al., 2013; Schwartz et al., 2014), is also required for endodermal and mesodermal differentiation (Fukusumi et al., 2008). The observed phenotypes in ESC and teratomas are all the more notable because we have significantly reduced but not eliminated m^6A.

Our findings suggest a model where m^6A serves as the necessary flexibility factor to counter balance epigenetic fidelity—a RNA “anti-epigenetics” (Figure 7F). m^6A marks a wide range of transcripts, including ESC fate determinants to limit their level of expression, and ensure their continual degradation so that cells can rapidly transition between gene expression programs. In ESC, m^6A is required for cells to rapidly exit the pluripotent state upon

differentiation. The inability to exit the stem cell state and continued proliferation upon insufficient m^6A offers a potential explanation for the association of FTO with human cancers (Loos and Yeo, 2013). METTL3 depletion also leads to elongation of the circadian clock (Fustin et al., 2013), suggesting a role for m^6A in resetting the transcriptome. In yeast, m^6A is active during meiosis (Clancy et al., 2002), where diploid gene expression programs are reset to generate haploid offspring. We propose that m^6A makes the transition between cell states possible by facilitating a reset mechanism between stages, as occurs in ESCs and likely other cell types. In contrast to epigenetic mechanisms that provide cellular memory of gene expression states, m^6A enforces the transience of genetic formation – helping cells to forget the past and thereby embrace the future.

EXPERIMENTAL PROCEDURES

For full details, see Extended Experimental Procedure.

Mouse cell culture and differentiation

J-1 murine embryonic stem cells were grown under typical feeder free ES cell culture conditions. For cardiomyocyte formation, mESCs were differentiated in cardiomyocyte differentiation media and scored on day 12. For neuron formation, mESCs were differentiated in MEF and ITSFn medium and scored after 10 days in ITSFn medium. For the cell proliferation assay 5000 cells where cultured in 24 well plates and the assay performed according to the manufacturer's protocol (MTT assay). For the single colony assays and Nanog staining, 1000 cells where cultured per well, on a six well plate. For alkaline phosphatase staining, cells were stained according to the manufacturer's protocol (Vector Blue Alkaline Phosphatase Substrate Kit).

hESCs cell culture, transfection and differentiation

H1 (WA01) cells were cultured in feeder-free conditions as described (Sigova et al., 2013). Stable hESC lines were created that expressed shMETTL3 RNA or scrambled shRNA by transfecting hESCs with plasmids encoding shMETTL3 or scrambled shRNA and a puromycin resistance gene. Cells were treated with puromycin for six days beginning two days after transfection. For each shRNA, two independent puromycin-resistant colonies were picked and expanded. Endodermal differentiation was then induced by Activin A, as described (Sigova et al., 2013). Day 2 and Day 4 of differentiation were measured from the time that Activin was added. Puromycin was removed from the media one day prior to endodermal differentiation.

RNA m^6A IP and m^6A methylation IP RNA-sequencing analysis

Libraries generated with iCLIP adaptors where separated by barcode, and perfectly matching reads were collapsed. Sequencing reads were mapped using TopHat (Trapnell et al., 2009). A non-redundant mm9 transcriptome was assembled from UCSC RefSeq genes, UCSC genes, and predictions from (Ulitsky et al., 2011) and (Guttman et al., 2011). For human datasets, the Ensembl genes (release 64) was used. Search for enriched peaks was performed by scanning each gene using 100-nucleotide sliding windows, and calculating an

enrichment score for each sliding window (Dominissini et al., 2012). HOMER software package (Heinz et al., 2010) was used for de novo discovery of the methylation motif.

CRISPR-mediated *Mettl3* knockout

gRNA sequences where chosen and designed a CRISPR design tool (Hsu et al., 2013). Plasmids for guide RNA were co-nucleofected, with a human codon optimized Cas9 expression plasmid and a plasmid with a puromycine resistance cassette. Cells were plated at low density for single colony isolation and selected single colonies tested by western blot for loss of protein.

Determination of m^6A levels

2D-TLC was performed as described by (Jia et al., 2011). For dot-blots, the indicated amounts of RNA were applied to the membrane and cross-linked by UV. The m^6A primary antibody was added at a concentration of 1:500. The membrane was incubated with the secondary antibody and exposed to an auto-radiographic film. m^6A RNA mass-spectrometry was performed as described in the Extended Experimental Procedures.

Dataset comparison

Mouse Pol II occupancy data, mRNA half life and Protein translation efficiency were obtained from (Ingolia et al., 2011; Rahl et al., 2010; Sharova et al., 2009). Plotting and statistical tests were performed in R. Multi-dimensional gene set enrichment analysis over DAVID Gene Ontology terms and stem cell gene sets (Wong et al., 2008) were performed using Genomica (Segal et al., 2003).

Teratoma generation and histopathology

Mettl3 wild type and mutant cells were subcutaneously injected into 8-week-old female SCID/Beige mice (Charles River). Four weeks after injection, the mice were euthanized and the tumors harvested. All animal studies were approved by Stanford University IACUC guidelines. For histological analysis, slides were stained with hematoxylin and eosin (H&E) or stained by immunohistochemistry (IHC) with VECTASTAIN ABC Kit and DAB Peroxidase Substrate Kit following the manufacturer's instructions. Analyses were performed by a boarded veterinary pathologist (DMB).

Supplementary Material

Refer to Web version on PubMed Central for supplementary material.

Acknowledgments

We thank C. He, C. Mason, S. Schwartz, A. Regev, J. M. Claycomb, N. Van Wittenberghe, B.D. Howard and members of the Chang and Giallourakis labs for discussions, and assistance. We thank H.E. Arda and S.K. Kim, for help with FACS analysis, and A. Memmelaar for his expertise in graphic arts. Supported by California Institute for Regenerative Medicine and NIH R01-CA118750 (H.Y.C.), the MGH Start-Up Funds and MGH ECOR grant 2013A051178 (C.C.G.), NIH grant DK090122 (A.C.M.), and the Eli and Edythe Broad Center of Regenerative Medicine and Stem Cell Research at UCLA Research Award (Y.X.). P.J.B. is the Kenneth G. and Elaine A. Langone Fellow of the Damon Runyon Cancer Research Foundation. Y.X. is an Alfred Sloan Foundation Research Fellow. H.Y.C. is an Early Career Scientist of the Howard Hughes Medical Institute.

References

Bodi Z, Zhong S, Mehra S, Song J, Graham N, Li H, May S, Fray RG. Adenosine Methylation in Arabidopsis mRNA is Associated with the 3′ End and Reduced Levels Cause Developmental Defects. Front Plant Sci. 2012; 3:48. [PubMed: 22639649]

Clancy MJ, Shambaugh ME, Timpte CS, Bokar JA. Induction of sporulation in Saccharomyces cerevisiae leads to the formation of N6-methyladenosine in mRNA: a potential mechanism for the activity of the IME4 gene. Nucleic Acids Res. 2002; 30:4509–4518. [PubMed: 12384598]

Dawlaty MM, Breiling A, Le T, Raddatz G, Barrasa MI, Cheng AW, Gao Q, Powell BE, Li Z, Xu M, et al. Combined deficiency of Tet1 and Tet2 causes epigenetic abnormalities but is compatible with postnatal development. Dev Cell. 2013; 24:310–323. [PubMed: 23352810]

Dawlaty MM, Ganz K, Powell BE, Hu YC, Markoulaki S, Cheng AW, Gao Q, Kim J, Choi SW, Page DC, et al. Tet1 is dispensable for maintaining pluripotency and its loss is compatible with embryonic and postnatal development. Cell Stem Cell. 2011; 9:166–175. [PubMed: 21816367]

Dominissini D, Moshitch-Moshkovitz S, Schwartz S, Salmon-Divon M, Ungar L, Osenberg S, Cesarkas K, Jacob-Hirsch J, Amariglio N, Kupiec M, et al. Topology of the human and mouse m6A RNA methylomes revealed by m6A-seq. Nature. 2012; 485:201–206. [PubMed: 22575960]

Dunn SJ, Martello G, Yordanov B, Emmott S, Smith AG. Defining an essential transcription factor program for naive pluripotency. Science. 2014; 344:1156–1160. [PubMed: 24904165]

Fu Y, He C. Nucleic acid modifications with epigenetic significance. Curr Opin Chem Biol. 2012; 16:516–524. [PubMed: 23092881]

Fukusumi Y, Naruse C, Asano M. Wtap is required for differentiation of endoderm and mesoderm in the mouse embryo. Dev Dyn. 2008; 237:618–629. [PubMed: 18224709]

Fustin JM, Doi M, Yamaguchi Y, Hida H, Nishimura S, Yoshida M, Isagawa T, Morioka MS, Kakeya H, Manabe I, et al. RNA-Methylation-Dependent RNA Processing Controls the Speed of the Circadian Clock. Cell. 2013; 155:793–806. [PubMed: 24209618]

Guttman M, Donaghey J, Carey BW, Garber M, Grenier JK, Munson G, Young G, Lucas AB, Ach R, Bruhn L, et al. lincRNAs act in the circuitry controlling pluripotency and differentiation. Nature. 2011; 477:295–300. [PubMed: 21874018]

Harcourt EM, Ehrenschwender T, Batista PJ, Chang HY, Kool ET. Identification of a selective polymerase enables detection of N(6)-methyladenosine in RNA. J Am Chem Soc. 2013; 135:19079–19082. [PubMed: 24328136]

Heinz S, Benner C, Spann N, Bertolino E, Lin YC, Laslo P, Cheng JX, Murre C, Singh H, Glass CK. Simple combinations of lineage-determining transcription factors prime cis-regulatory elements required for macrophage and B cell identities. Mol Cell. 2010; 38:576–589. [PubMed: 20513432]

Horiuchi K, Kawamura T, Iwanari H, Ohashi R, Naito M, Kodama T, Hamakubo T. Identification of Wilms' tumor 1-associating protein complex and its role in alternative splicing and the cell cycle. J Biol Chem. 2013

Hsu PD, Scott DA, Weinstein JA, Ran FA, Konermann S, Agarwala V, Li Y, Fine EJ, Wu X, Shalem O, et al. DNA targeting specificity of RNA-guided Cas9 nucleases. Nat Biotechnol. 2013; 31:827–832. [PubMed: 23873081]

Ingolia NT, Lareau LF, Weissman JS. Ribosome profiling of mouse embryonic stem cells reveals the complexity and dynamics of mammalian proteomes. Cell. 2011; 147:789–802. [PubMed: 22056041]

Jia G, Fu Y, Zhao X, Dai Q, Zheng G, Yang Y, Yi C, Lindahl T, Pan T, Yang YG, et al. N6-methyladenosine in nuclear RNA is a major substrate of the obesity-associated FTO. Nat Chem Biol. 2011; 7:885–887. [PubMed: 22002720]

Kang HJ, Jeong SJ, Kim KN, Baek IJ, Chang M, Kang CM, Park YS, Yun CW. A novel protein, Pho92, has a conserved YTH domain and regulates phosphate metabolism by decreasing the mRNA stability of PHO4 in Saccharomyces cerevisiae. Biochem J. 2014; 457:391–400. [PubMed: 24206186]

Lin N, Chang KY, Li Z, Gates K, Rana ZA, Dang J, Zhang D, Han T, Yang CS, Cunningham TJ, et al. An Evolutionarily Conserved Long Noncoding RNA TUNA Controls Pluripotency and Neural Lineage Commitment. Mol Cell. 2014; 53:1005–1019. [PubMed: 24530304]

Liu J, Yue Y, Han D, Wang X, Fu Y, Zhang L, Jia G, Yu M, Lu Z, Deng X, et al. A METTL3-METTL14 complex mediates mammalian nuclear RNA N6-adenosine methylation. Nat Chem Biol. 2014; 10:93–95. [PubMed: 24316715]

Liu N, Parisien M, Dai Q, Zheng G, He C, Pan T. Probing N6-methyladenosine RNA modification status at single nucleotide resolution in mRNA and long noncoding RNA. Rna. 2013

Loewer S, Cabili MN, Guttman M, Loh YH, Thomas K, Park IH, Garber M, Curran M, Onder T, Agarwal S, et al. Large intergenic non-coding RNA-RoR modulates reprogramming of human induced pluripotent stem cells. Nat Genet. 2010; 42:1113–1117. [PubMed: 21057500]

Loh KM, Lim B. A precarious balance: pluripotency factors as lineage specifiers. Cell Stem Cell. 2011; 8:363–369. [PubMed: 21474100]

Loos RJ, Yeo GS. The bigger picture of FTO-the first GWAS-identified obesity gene. Nat Rev Endocrinol. 2013

Meyer KD, Jaffrey SR. The dynamic epitranscriptome: N6-methyladenosine and gene expression control. Nat Rev Mol Cell Biol. 2014; 15:313–326. [PubMed: 24713629]

Meyer KD, Saletore Y, Zumbo P, Elemento O, Mason CE, Jaffrey SR. Comprehensive analysis of mRNA methylation reveals enrichment in 3′ UTRs and near stop codons. Cell. 2012; 149:1635–1646. [PubMed: 22608085]

Montserrat N, Nivet E, Sancho-Martinez I, Hishida T, Kumar S, Miquel L, Cortina C, Hishida Y, Xia Y, Esteban CR, et al. Reprogramming of human fibroblasts to pluripotency with lineage specifiers. Cell Stem Cell. 2013; 13:341–350. [PubMed: 23871606]

Neff AT, Lee JY, Wilusz J, Tian B, Wilusz CJ. Global analysis reveals multiple pathways for unique regulation of mRNA decay in induced pluripotent stem cells. Genome Res. 2012; 22:1457–1467. [PubMed: 22534399]

Niu Y, Zhao X, Wu YS, Li MM, Wang XJ, Yang YG. N6-methyl-adenosine (m6A) in RNA: an old modification with a novel epigenetic function. Genomics Proteomics Bioinformatics. 2013; 11:8–17. [PubMed: 23453015]

Rahl PB, Lin CY, Seila AC, Flynn RA, McCuine S, Burge CB, Sharp PA, Young RA. c-Myc regulates transcriptional pause release. Cell. 2010; 141:432–445. [PubMed: 20434984]

Schnerch A, Cerdan C, Bhatia M. Distinguishing between mouse and human pluripotent stem cell regulation: the best laid plans of mice and men. Stem Cells. 2010; 28:419–430. [PubMed: 20054863]

Schwartz S, Agarwala SD, Mumbach MR, Jovanovic M, Mertins P, Shishkin A, Tabach Y, Mikkelsen TS, Satija R, Ruvkun G, et al. High-resolution mapping reveals a conserved, widespread, dynamic mRNA methylation program in yeast meiosis. Cell. 2013; 155:1409–1421. [PubMed: 24269006]

Schwartz S, Mumbach MR, Jovanovic M, Wang T, Maciag K, Bushkin GG, Mertins P, Ter-Ovanesyan D, Habib N, Cacchiarelli D, et al. Perturbation of m6A Writers Reveals Two Distinct Classes of mRNA Methylation at Internal and 5′ Sites. Cell Rep. 2014; 8:284–296. [PubMed: 24981863]

Segal E, Shapira M, Regev A, Pe'er D, Botstein D, Koller D, Friedman N. Module networks: identifying regulatory modules and their condition-specific regulators from gene expression data. Nat Genet. 2003; 34:166–176. [PubMed: 12740579]

Sharova LV, Sharov AA, Nedorezov T, Piao Y, Shaik N, Ko MS. Database for mRNA half-life of 19 977 genes obtained by DNA microarray analysis of pluripotent and differentiating mouse embryonic stem cells. DNA Res. 2009; 16:45–58. [PubMed: 19001483]

Shu J, Wu C, Wu Y, Li Z, Shao S, Zhao W, Tang X, Yang H, Shen L, Zuo X, et al. Induction of pluripotency in mouse somatic cells with lineage specifiers. Cell. 2013; 153:963–975. [PubMed: 23706735]

Sibbritt T, Patel HR, Preiss T. Mapping and significance of the mRNA methylome. Wiley Interdiscip Rev RNA. 2013; 4:397–422. [PubMed: 23681756]

Sigova AA, Mullen AC, Molinie B, Gupta S, Orlando DA, Guenther MG, Almada AE, Lin C, Sharp PA, Giallourakis CC, et al. Divergent transcription of long noncoding RNA/mRNA gene pairs in embryonic stem cells. Proc Natl Acad Sci U S A. 2013; 110:2876–2881. [PubMed: 23382218]

Trapnell C, Pachter L, Salzberg SL. TopHat: discovering splice junctions with RNA-Seq. Bioinformatics. 2009; 25:1105–1111. [PubMed: 19289445]

Ulitsky I, Shkumatava A, Jan CH, Sive H, Bartel DP. Conserved function of lincRNAs in vertebrate embryonic development despite rapid sequence evolution. Cell. 2011; 147:1537–1550. [PubMed: 22196729]

Wang X, Lu Z, Gomez A, Hon GC, Yue Y, Han D, Fu Y, Parisien M, Dai Q, Jia G, et al. N6-methyladenosine-dependent regulation of messenger RNA stability. Nature. 2014a; 505:117–120. [PubMed: 24284625]

Wang Y, Li Y, Toth JI, Petroski MD, Zhang Z, Zhao JC. N6-methyladenosine modification destabilizes developmental regulators in embryonic stem cells. Nat Cell Biol. 2014b; 16:191–198. [PubMed: 24394384]

Wong DJ, Liu H, Ridky TW, Cassarino D, Segal E, Chang HY. Module map of stem cell genes guides creation of epithelial cancer stem cells. Cell Stem Cell. 2008; 2:333–344. [PubMed: 18397753]

Young RA. Control of the embryonic stem cell state. Cell. 2011; 144:940–954. [PubMed: 21414485]

Zheng G, Dahl JA, Niu Y, Fedorcsak P, Huang CM, Li CJ, Vagbo CB, Shi Y, Wang WL, Song SH, et al. ALKBH5 is a mammalian RNA demethylase that impacts RNA metabolism and mouse fertility. Mol Cell. 2013; 49:18–29. [PubMed: 23177736]

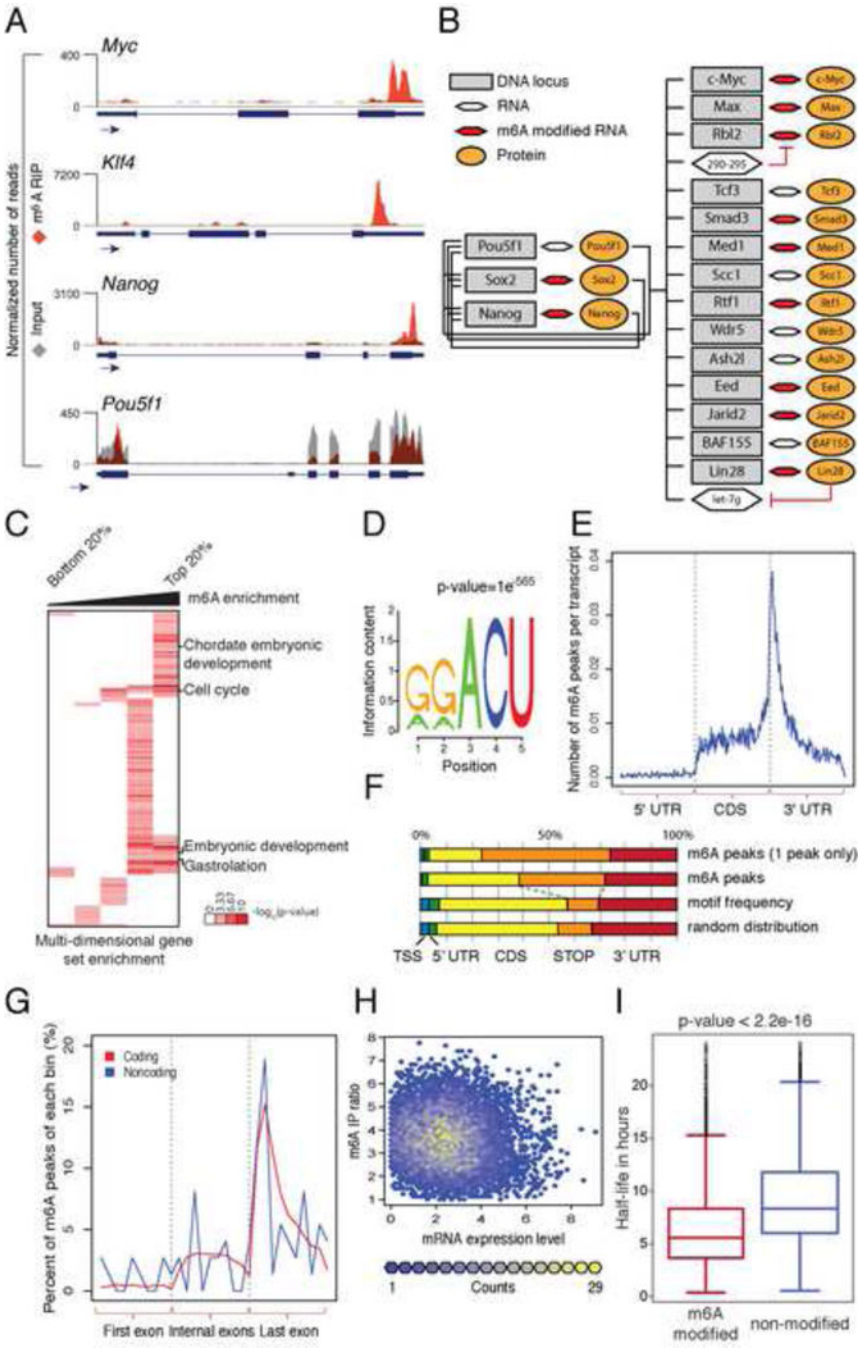

Figure 1. Topology and characterization of m^{6}A target genes

(A) UCSC Genome browser plots of m^{6}A-seq reads along indicated mRNAs. Grey reads are from non-immunoprecipitated input libraries and red reads from anti-m^{6}A immunoprecipitation libraries. The y-axis represents normalized number of reads. Blue thick boxes represent the open reading frame while the blue line represents the untranslated regions. See also Figure S1A and Table S1 and S2. **(B)** Model of genes involved in maintenance of stem cell state (adapted from Young et al., 2011). Red hexagons represent modified mRNAs. **(C)** Heatmap with log10 (p-vlaue) of gene set enrichment analysis for

m^6A modified genes. **(D)** Sequence motif identified after analysis of m^6A enrichment regions. See also Figure S1B, S1C. **(E)** Normalized distribution of m^6A peaks across 5′ UTR, CDS and 3′UTR of mRNAs for peaks common to all samples. **(F)** Graphical representation of frequency of m^6A peaks and methylation motifs in genes, divided into 5 distinct regions. **(G)** Distribution of m^6A peaks across the length of mRNAs (n=5070) and non-coding RNAs (n=51). See also Figure S1D, S1E, S1F, S1G and S1H. **(H)** Scatter plot representation of m^6A enrichment score (on the X axis) and gene expression level (on the Y axis) for each m^6A peak. See also Figure S1I. **(I)** Box plot representing the half-life for transcripts with at least one modification site and transcripts with no modification site identified. See also figure S1J and S1K.

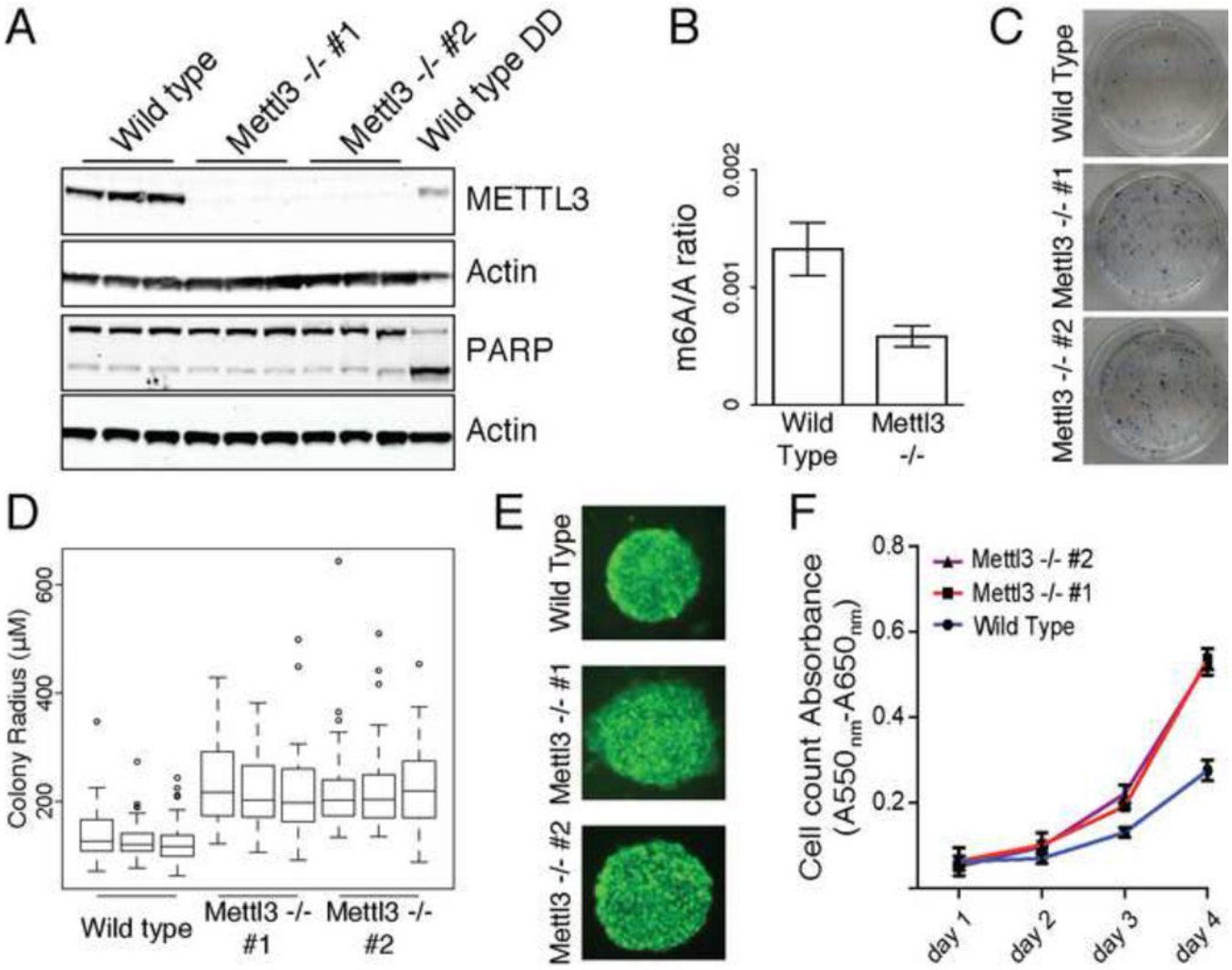

Figure 2. Characterization of Mettl3 knock out cells

(A) Western blot for Mettl3 and PARP in wild type and two cell lines with CRISPR induced loss of protein (DD: DNA damaging agent). Actin is used as loading control. See also Figure S2A. **(B)** m^6A ratio determined by 2D-TLC in wild type and Mettl3 KO. Error bars represent standard deviation of 3 biological replicates in all panels. See also Figure S2B and S2C. **(C)** Alkaline phosphatase staining of wild type and Mettl3 knock out cells. See also Figure S2D and S2E. **(D)** Box plot representation of colony radius for wild type and Mettl3 mutant cells. Experiments were performed in triplicate, with at least 50 colonies measured for each replicate. **(E)** Nanog staining of colonies of wild type and two cell lines with CRISPR induced loss of protein. **(F)** Cell proliferation assay of wild type and two cell lines with CRISPR induced loss of Mettl3 protein. See also Figure S2F, S2G and S2H.

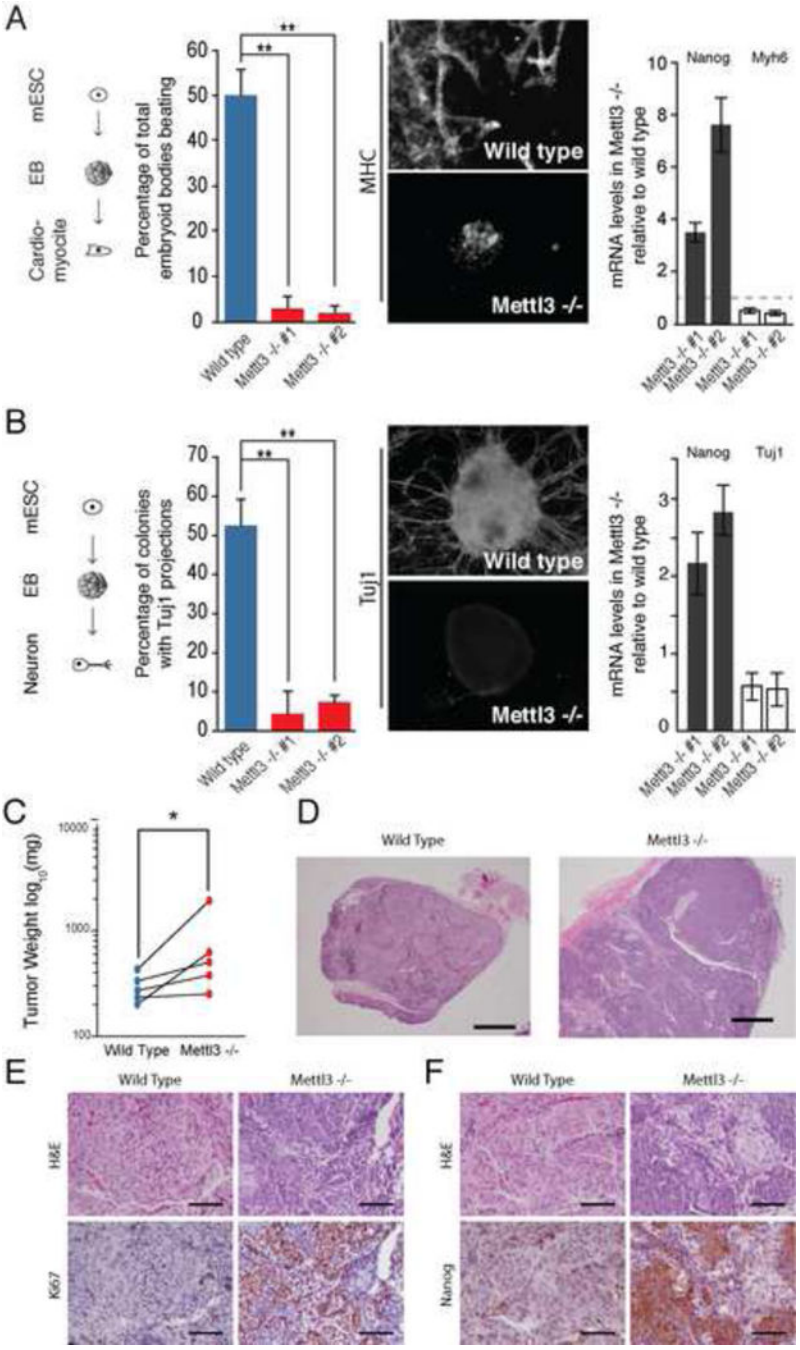

Figure 3. Mettl3 loss of function impairs ESC ability to differentiate

(A) Percentage of embryoid bodies with beating activity in Mettl3 KO and wild type control cells (right panel). Representative images of bodies stained for MHC and DAPI (center panel) and mRNA levels of Nanog and Myh6, measured by qRT-PCR, in Mettl3 KO cells in relation to wild type control cells. Error bars, standard deviation of 3 biological replicates in all panels. * represents p-value < 0.05, t-test (2 tailed). See also Movie S1 and S2. **(B)** Percentage of colonies with Tuj1 projections in Mettl3 KO and wild type control cells (right panel). Representative images of bodies stained for Tuj1 and DAPI (center panel) and

mRNA levels of Nanog and Tuj1, measured by qRT-PCR, in Mettl3 KO cells in relation to wild type control cells. * represents p-value < 0.05, t-test (2 tailed). **(C)** Weight differences between teratomas generated from wild type and Mettl3 knock out cells. Tumors are paired by animal (n=5). **(D)** Representative sections of teratomas stained with hematoxylin and eosin at low magnification. Bar=1000 μm. See also Figure S3A. **(E and F)** Immunohistochemistry with antibody against Ki67 **(E)** and with antibody against Nanog **(F)**. Bar represents 100 μm. See also Figure S3B.

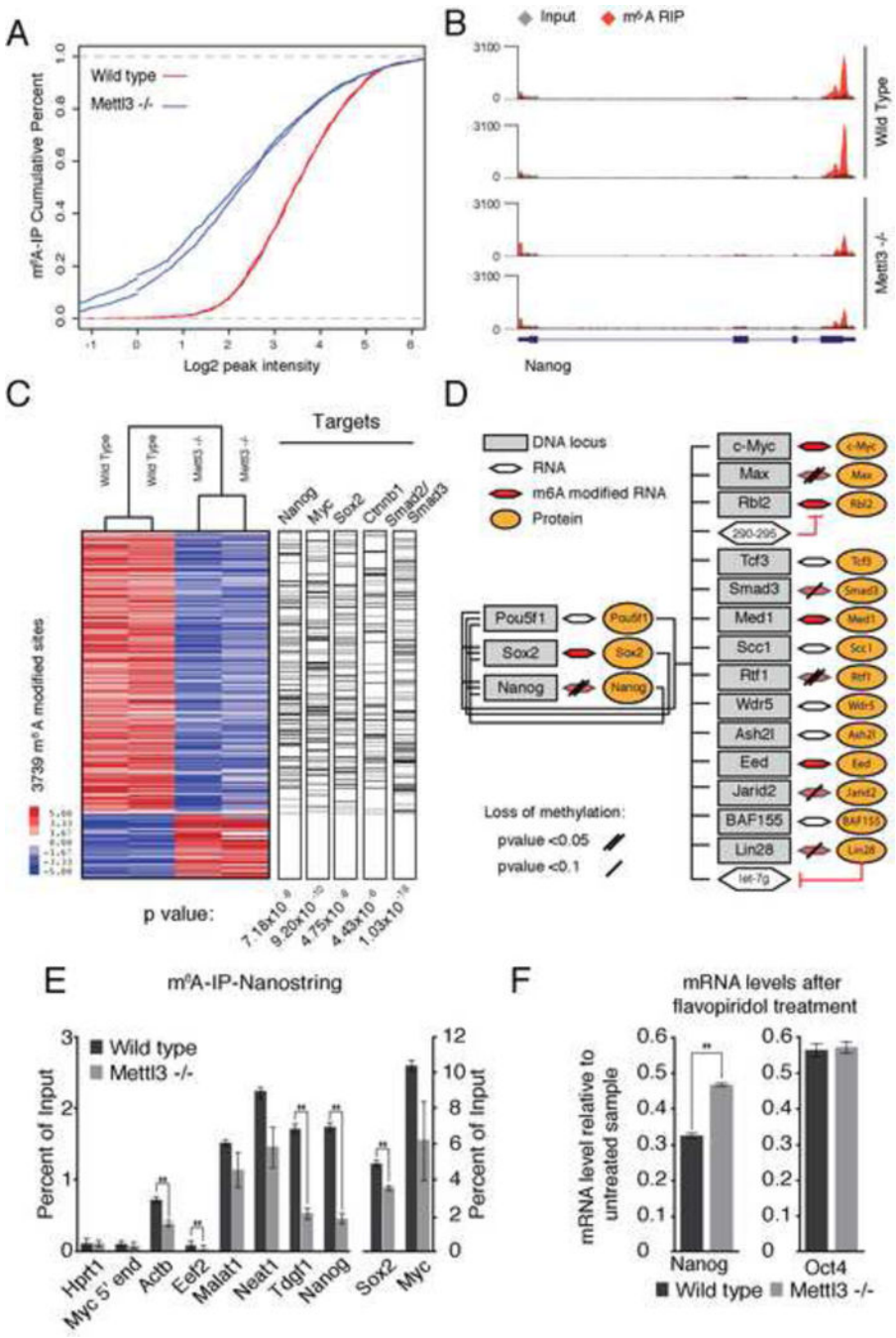

Figure 4. Impact of loss of Mettl3 on the mESC methylome

(A) Cumulative distribution function of log2 peak intensity of m^{6}A modified sites. **(B)** Sequencing read density for input (grey) vs. in m^{6}A IP (red) for *Nanog*. Y-axis represents normalized number of reads. Gene model as in Figure 1A. **(C)** Heatmap representing IP enrichment values for peaks with statistically significant difference between wild type and Mettl3 mutant. Bar to the right represent genes in each dataset with a >1.5 fold decrease in IP enrichment values. **(D)** Model of genes involved in maintenance of stem cell state (adapted from Young et al., 2011), representing transcripts with loss of m^{6}A modification in

Mettl3 −/− cells. **(E)** Percentage of input recovered after m^6A IP measured by Nanostring for each mRNA. Error bars, standard deviation of 2 biological replicates. *, p-value < 0.05, t-test (2 tailed). **(F)** mRNA levels of Nanog and Oct4, measured by qRT-PCR, after PolII inhibition relative to untreated sample in wild type and Mettl3 KO cells. Error bars, standard deviation of 3 biological replicates. *, p-value < 0.05, t-test (2 tailed).

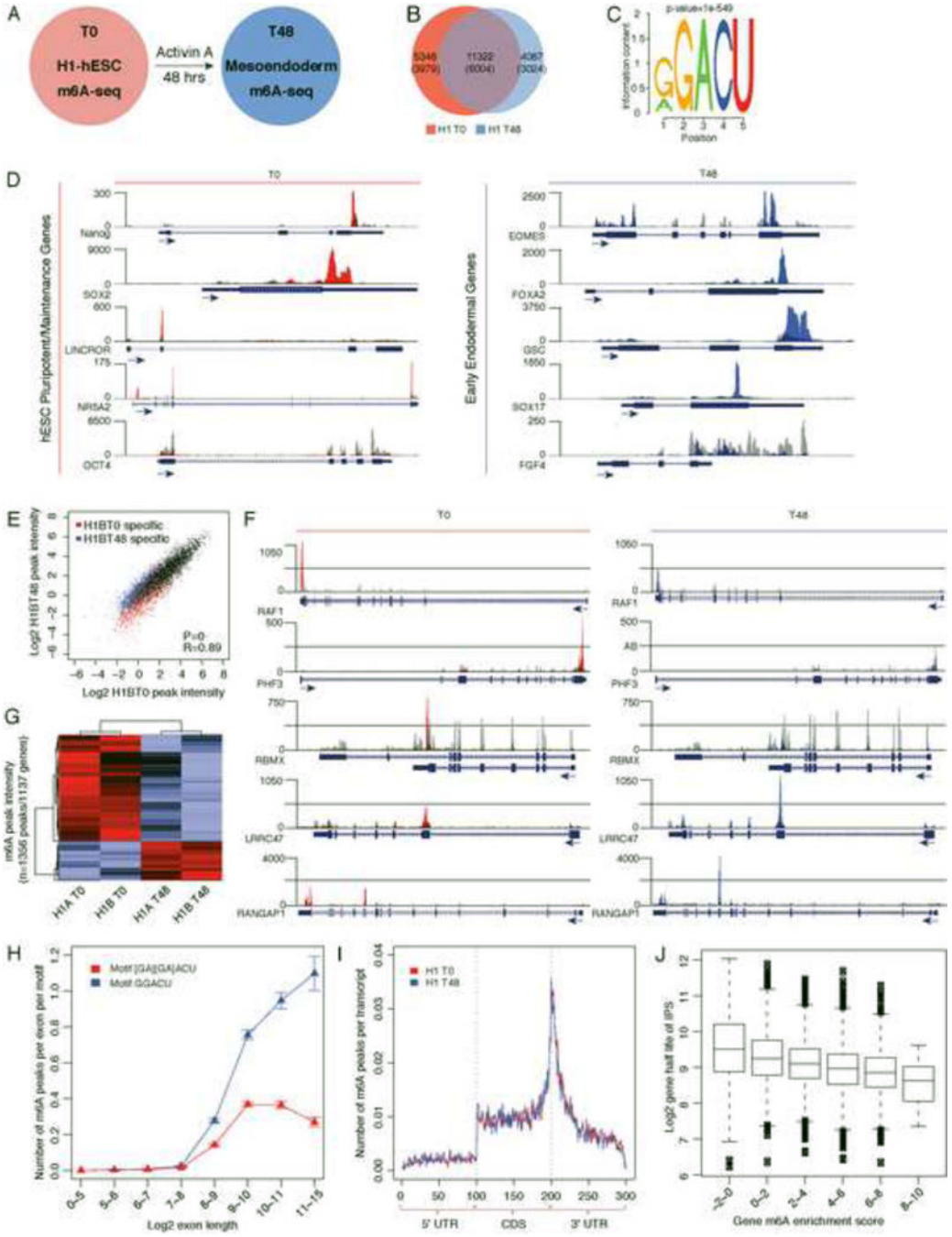

Figure 5. m^{6}A-seq profiling of hESC during endoderm differentiation

(A) m^{6}A-seq was performed in resting (undifferentiated) human H1-ESCs (T0) and after 48hrs of Activin A induction towards endoderm (mesoendoderm) (T48). **(B)** Venn diagram of the overlap between high-confidence T0 and T48 m6A peaks. The number of genes in each category is shown in parenthesis. See also Table S3 and S4. **(C)** Sequence motif identified after analysis of m^{6}A enrichment regions. **(D)** UCSC Genome browser plots of m^{6}A-seq reads along indicated RNAs. Grey reads are from non-immunoprecipitated control input libraries and red (T0) or blue (T48) reads are from anti-m^{6}A immunoprecipitation

libraries. Y-axis represents normalized number of reads; X-axis is genomic coordinates. Key regulators of stem cell maintenance (left) and master regulators of endoderm differentiation (right) are represented. See also Figure S4A. **(E)** Scatterplot of m^6A peak intensities between two different time points (T0 versus T48) of the same biological replicate with only "high-confidence" T0 or T48 specific peaks supported by both biological replicates highlighted. **(F)** UCSC Genome browser plots of m^6A-seq reads along indicated mRNAs in undifferentiated (T0) versus differentiated cells (T48). The grey reads are from non-immunoprecipitated control input libraries. The red and blue reads are from the anti-m^6A RIP of T=0 and T=48 samples respectively. **(G)** Differential intensities of m^6A peaks (DMPIs) identify hESC cell states T0 vs T48hrs. Z score scaled Log2 peak intensities of DMPIs are color-coded according to the legend. The peaks and samples are both clustered by average linkage hierarchical clustering using 1-Pearson correlation coefficient of log2 peak intensity as the distance metric. **(H)** Number of peaks per exon normalized by the number of motifs (on sense strand) in the exon. The error bars represent standard deviations from 1000 times of bootstrapping. **(I)** The normalized distribution of m^6A peaks across the 5′UTR, CDS, and 3′UTR of mRNAs for T0 and T48 m^6A peaks. See also Figure S4B, S4C and S4D. **(J)** Box plot representing the half-life for transcripts, with transcripts separated according to enrichment score. See also Figure S4E, S4F and S4G.

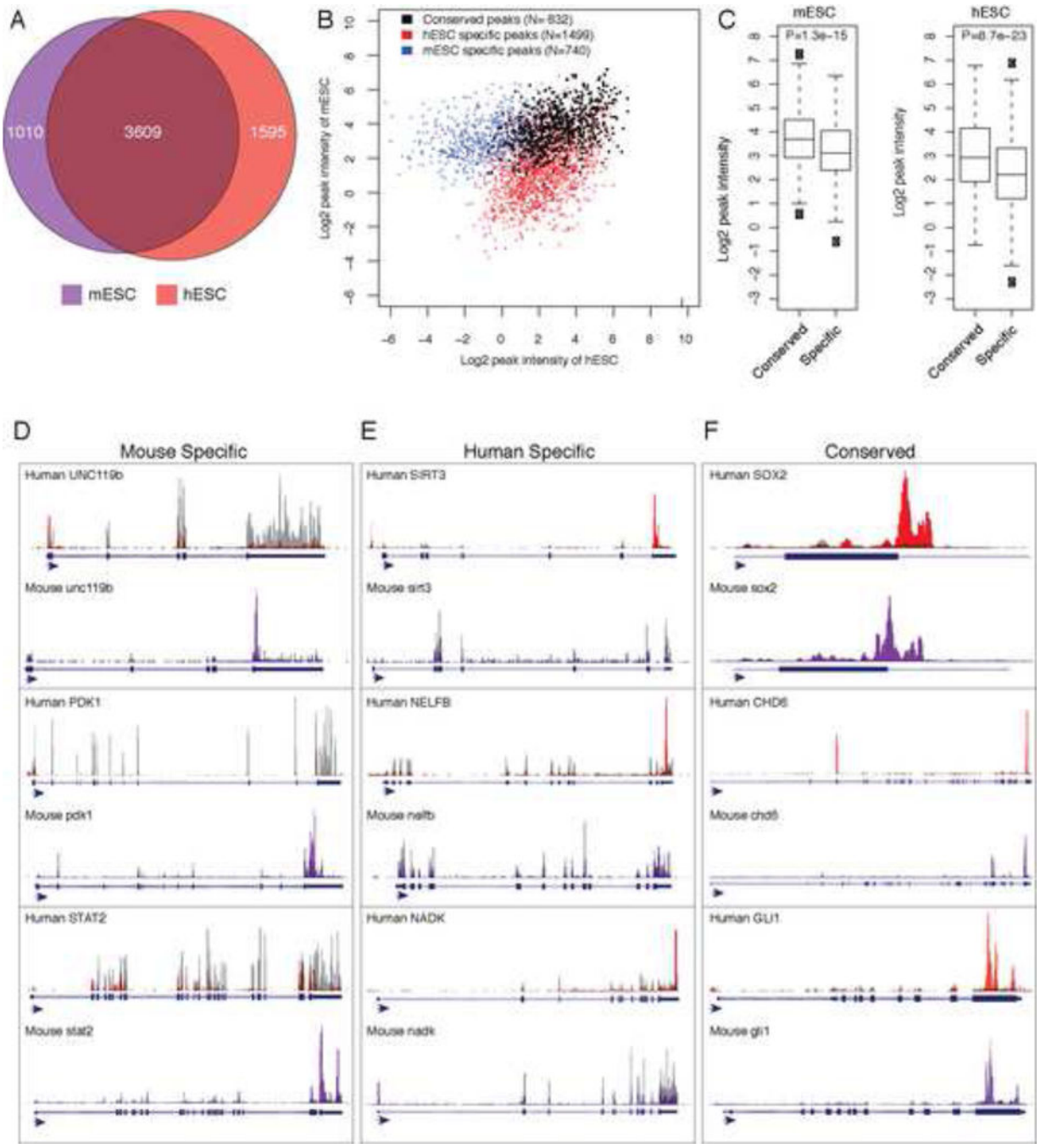

Figure 6. Evolutionary conservation and divergence of the m^{6}A epi-transcriptomes of human and mouse ESCs

(A) Venn diagram showing a 62% overlap between methylated genes in *M. musculus* (purple) and *H. sapiens* (red) embryonic stem cells (p value= $3.5 \times 10^{-92;}$ Fisher exact test). See also Table S5 and S6. **(B)** The m^{6}A peaks that could be mapped to orthologous genomic windows between mouse and human were identified. The intensities of m^{6}A-seq signals in human and mouse ESCs were shown for m^{6}A peaks found to be unique in mouse (blue), unique in human (red), and conserved between human and mouse (black). **(C)** Boxplot of

peak intensities of m^6A sites conserved ("common") or not conserved ("specific") in mouse and human ESCs. (p values=1.3×10^{-15} and 8.7×10^{-23} respectively). **(D to F)** UCSC Genome browser plots of m^6A-seq reads along indicated mRNAs. The grey reads are from non-immunoprecipitated control input libraries and the purple and red reads are from the anti-m^6A RIP of mESCs and hESCs (T0) respectively. **(D)** Mouse-specific m^6A modifications are represented. **(E)** Human-specific m^6A modifications ESCs are represented. **(F)** Conserved m^6A modifications at gene and site level are represented. Genes such CHD6 have a conserved m^6A peak location at its 3′UTR as well as mouse and human specific m^6A peaks at conserved but distinct exons.

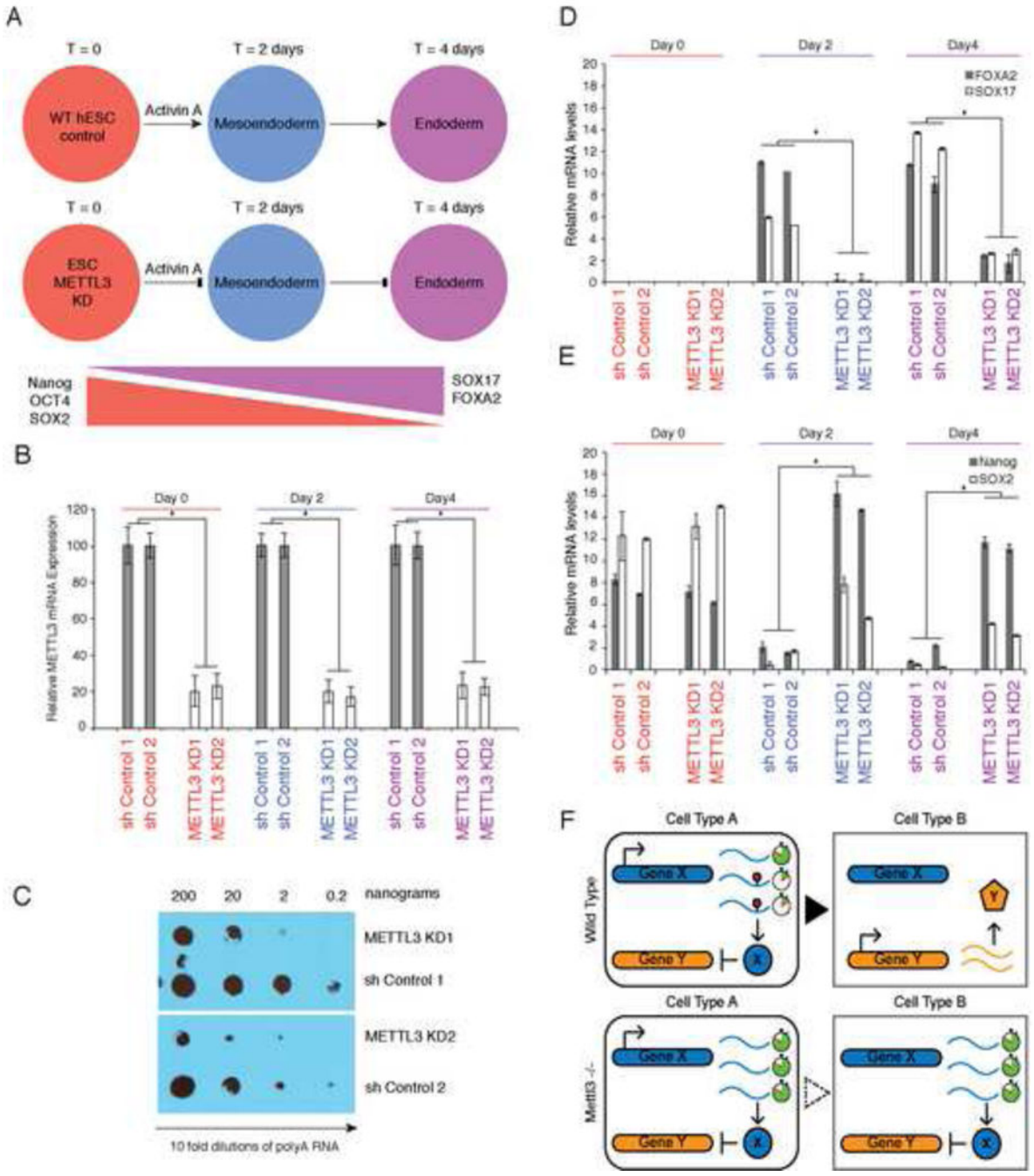

Figure 7. METTL3 is required for normal human ESC endoderm differentiation. Model of METTL3 function(s)

(A) hESC cells were transfected with anti-METTL3 shRNA (KD) as well control shRNA and stable hESC colonies were obtained after drug selection. Two independent clones were subjected to endodermal differentiation with Activin A and examined at various indicated time points. A schematic of the trends of gene expression for indicated markers of stem maintenance and endoderm differentiation is also shown. See also figure S5A. **(B)** Levels of *METTL3* mRNA in hESC cells with control shRNA versus anti-METTL3 shRNA (KD)

across the three indicated time points during endodermal differentiation (n=2 independent generated ES cell knockdown and control clones shown). In all panels, Error bars represent standard deviation across 3 replicates per time point; *, p value<0.05 t-test (2 tailed) between different clones. See also Figure S5B. **(C)** Anti-m^{6}A dot blot was performed on 10x fold dilutions of polyA selected RNA from hESC cells derived from control shRNA versus anti-METTL3 shRNA clones. See also Figure S5C. **(D and E)** mRNA levels of endodermal and stem maintenance/marker genes. qRT-PCR was performed on indicated genes and time points (n=2 independently generated ES cell knockdown and control clones shown). See also Figure S5D. **(F)** Model: m^{6}A marks transcripts for faster turn-over. Upon transition to new cell fate, m^{6}A marked transcripts are readily removed to allow the expression of new gene expression networks. In the absence of m^{6}A, the unwanted presence of transcripts will disturb the proper balanced required for cell fate transitions.